Combined molecular dynamics–micromechanics methods to predict Young's modulus of fullerene-reinforced polymer composites

Razie Izadi, Ali Nayebi, Esmaeal Ghavanloo*

School of Mechanical Engineering, Shiraz University, Shiraz 71963-16548, Iran

Abstract

In this paper, a multiscale method is developed to predict Young's modulus of Fullerene-Reinforced Polymer Nanocomposites (FRPNs). Poly methyl methacrylate (PMMA) is chosen as the polymer matrix while C_{60} fullerene is considered as the reinforcement. First, molecular dynamics (MD) simulations are conducted to calculate the Young modulus of nanocomposite unit cell with different weight fractions of fullerene. Then, a micromechanics model for a composite with multi-inclusion reinforcements is developed based on the extension of the Mori-Tanaka model and generalized Eshelby's results. Numerical results obtained from the proposed micromechanics model are compared with those calculated from the MD simulations and good agreement is achieved. In addition, we propose an extension for the Halpin-Tsai model to predict Young's modulus of the FRPNs.

Keywords: Nanocomposite; Fullerene; Mechanical properties; Micromechanics model

1. Introduction

In recent years, there has been a growing interest in the application of polymer materials reinforced with nanostructures, in both industrial and scientific fields [1]. Fullerenes and other carbon nanostructures such as nanotubes and graphene sheets can be used as reinforcements of the polymer composites [2-4]. According to experimental researches, the incorporation of the fullerene into polymer matrices can significantly enhance their mechanical properties [5-10].

Computational modeling of the FRPNs enables parametric study of nanocomposites to assist the design of these materials for practical applications. Among various computational approaches, molecular dynamics simulation is considered to be a powerful tool to produce reliable results in material modeling. Recently, more attention has been paid to the investigation of the FRPNs through the MD simulations. The first attempt was provided by Adnan et al. [11] to elucidate the influence of filler size on elastic properties of fullerene reinforced polyethylene nanocomposites. However, in their investigation, fullerenes were modeled as rigid solid inclusions. Using the MD simulations, Ferdous et al. [12] investigated the effects of reinforcement dispersion and the strength of filler and matrix interface on the mechanical

* Corresponding author.

Tel.: +98-7136133251, Fax: +98 7136473511

E-mail: ghavanloo@shirazu.ac.ir (E. Ghavanloo)

properties of the FRPNs. They also proposed a finite element model and considered both interphase and interface regions around the fullerene. The effects of fullerene on the thermo-mechanical properties of Araldite LY 5052/Aradur HY 5052 cross-linked resin epoxy were studied by Jeyranpour et al. [13]. In another study, the elastic properties of high density polyethylene reinforced by fullerene and graphene fillers was studied by Lu et al [14] using the MD simulations. Recently, Giannopoulos [15] proposed a combined MD simulation and finite element method for predicting the elastic properties of the fullerene reinforced nylon-12. In another study, employing the MD simulations, Izadi et al. [16] estimated the elastic properties of polymer nanocomposites reinforced with C_{60} fullerene and $C_{60}@C_{240}$ carbon onion. More recently, thermo-elastic response of PMMA matrix reinforced with C_{240} was investigated using combination of MD simulations and the finite element method [17].

Although the MD simulations have usually been utilized in modeling the nanocomposites, these simulations are inherently time consuming and computationally expensive. To overcome the mentioned limitation, various combined MD simulations-micromechanics methods have been developed in the literature [18-20]. However, combined MD simulations-micromechanics methods for fullerene reinforced polymer composites have not been presented so far. In this study, we developed a multiscale method, which combines the MD simulations with a continuum micromechanics. First, the Young modulus of various FRPCs with different weight fractions of the C_{60} is obtained using the MD simulations. The Materials Studio software is used to perform the MD simulations. Then, the interphase region is distinguished around the fullerene molecule and its effective stiffness is calculated. A micromechanics model is developed for a non-dilute composite with a multi inclusion reinforcement based on the generalized Eshelby's results with the assumptions of the Mori-Tanaka approach. The developed micromechanics model is used to predict the elastic properties of unit cells. In addition, the results obtained from the MD simulations are used to extend the Halpin-Tsai micromechanics model.

2. Molecular modeling and simulations

2.1 Fullerene-reinforced polymer composites

In this work, the MD simulations are conducted using the simulation package Material Studio. In addition, the Condensed Phase Optimized Molecular Potential for Atomistic Simulation Studies (COMPASS) is employed to describe inter- and intra-atomic interactions. To control temperature and pressure of the system, the Nose-Hoover thermostat [21] and the Berendsen barostat [22] are used respectively. In addition, the velocity-Verlet integration algorithm is employed to integrate the equations of motion, with a time step of 1 fs and a potential cutoff of 1.5 nm. Furthermore, periodic boundary conditions are imposed in all directions of the nanocomposite unit cells. To construct the nanocomposite unit cells, a C_{60} fullerene is placed at the center of the unit cell and the Poly methyl methacrylate (PMMA) with 10 monomers is dispersed

uniformly within the cell in non-overlapping positions. Here, we construct four nanocomposite unit cells with various weight fractions of C_{60} (1, 2, 3 and 4 wt%). The total energy of the unit cells is minimized by adopting the smart algorithm which is a cascade of the steepest descent, adjusted basis set Newton-Raphson, and quasi-Newton methods. Then, the unit cells are relaxed at 500 K in an *NVT* ensemble for 300 ps. Subsequently, for 500 ps, they are subjected to an *NPT* ensemble with a temperature of 500 K and a pressure of 1 atm. Finally, the unit cells are equilibrated at ambient temperature and pressure, adopting an NPT ensemble at 1 atm. and 298 K for 500 ps. After construction of the cells, the deformation of the unit cells under uniaxial tension/compression and pure shear strains is studied. More details on the MD simulations are provided in Ref. [16]. Using the Voigt-Reuss-Hill approach, the values of Young's modulus of C_{60}/PMMA nanocomposites with various weight fractions are calculated and listed in Table 1 (Details of the calculation are given in Ref. [16]).

Table 1. Effective Young's modulus of C_{60}/PMMA nanocomposite cells with various weight fractions

Carbon filler	Percent of Concentration	Young's Modulus (GPa)
C_{60}	1	3.298
C_{60}	2	3.313
C_{60}	3	3.438
C_{60}	4	3.774

2.2. Young's modulus of dense interphase

Formation of an ordered layer around a nanofiller embedded in a polymer nanocomposite was proven through several experiments and MD simulations [23, 24]. This polymer layer has higher density and elastic properties than the amorphous bulk polymer. This layer is commonly referred as interphase. Characterization of interphase is usually performed through MD simulations. Several studies suggest that the enhancement of the mechanical properties of nanocomposites is mainly provided by the interphase [25]. In the present paper, a novel method is proposed for the calculation of Young's modulus of the interphase region. The idea of proposed method is based on the fact that Young's modulus of the PMMA polymer is directly related to its density [26]. For the calculation of interphase elastic properties, at the first step, the average density of interphase region, $\bar{\rho}$, can be estimated via the normalized density of polymer near the fullerene, $g(r)=\rho(r)/\rho_0$, which is plotted in Fig. 1 for one case as an instance. As shown in the figure, polymer atoms appear at a radius of 5.85 Å from the center of the fullerene. The existence of the fullerene perturbs the density profile of the surrounding polymer. Although the density perturbation is sensed until 27 Å distant from the fullerene center, the main disturbance is observed up to approximately 14.5 Å. Therefore, the interphase is considered as a spherical shell with its inner and outer radii equal to r_1=5.85 Å and r_2=14.5 Å, respectively. The average density of interphase region can be calculated by the following relation

$$\bar{\rho} = \frac{3\int_{r_1}^{r_2} r^2 g(r)\rho_0 dr}{r_2^3 - r_1^3} \tag{1}$$

where ρ_0 is the density of bulk polymer. Using Eq. (1) and setting $\rho_0 = 1.11$ g/cm^3, we obtain $\bar{\rho} = 1.16$ g/cm^3. Although it is not shown here, the average density of interphase region is not sensitive to the weight fraction of C_{60}. After estimating the density of interphase region, a polymer unit cell with the density of interphase region is constructed and its Young's modulus is determined. The calculated value of the interphase Young's modulus is 4.7 GPa.

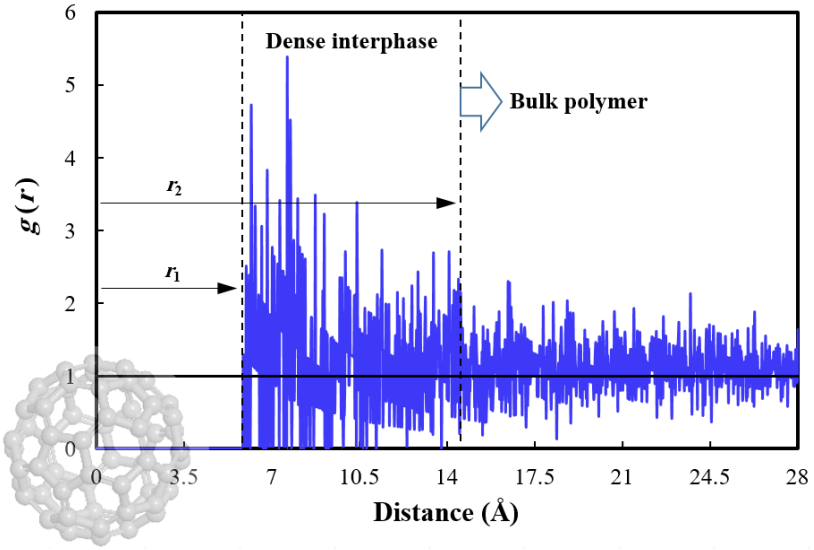

Fig. 1. Variations of the normalized density of polymer in the representative volume element (RVE) with 2 wt% of C_{60}.

2.3. Young's modulus of isolated C_{60}

Several researches have been conducted to estimate the Young modulus of the isolated C_{60} molecule using different approaches such as the MD simulations, the Mont Carlo simulations, molecular mechanics and finite element analysis. Different values have been reported in the literature ranging from 1.1 to 5.5 TPa [27-30]. For the estimation of Young's modulus of C_{60} molecule, various equivalent continuum structures such as spherical shell and solid sphere can be considered. In the present paper, we have considered both cases in the evaluation of micromechanics model. The values of Young's modulus, which will be used in our micromechanical model, are listed in Table 2.

Table 2. Effective Young's modulus of C_{60}

Equivalent continuum structure	Young's Modulus (GPa)
Spherical shell	2.1
Solid sphere	1.2

3. Micromechanics Model

Although the MD simulations are very useful tools for the characterization of polymer nanocomposites, they are computationally expensive and time-consuming. Therefore, development of a micromechanics model, which can effectively predict the mechanical properties of nanocomposites, can be quite beneficial. In this section, a micromechanics model is developed for a composite with multi-layer inclusions based on the extension of Mori-Tanaka model and generalized Eshelby's results proposed by Nemmat-Nasser and Hori [31]. Two main issues play basic roles in the development of our micromechanics model: 1) equivalent homogenous solid and 2) generalization of Eshelby's results. Prior to the description of the developed micromechanics model, named as "Extended Mori-Tanaka" model, these two issues are explained in the next subsections.

3.1. Equivalent homogeneous RVE and Eshelby's Tensor

Consider a finite homogeneous linear elastic solid V with elasticity tensor $\mathbf{C}$, which contains a homogeneous linear elastic inclusion Ω with elasticity tensor $\mathbf{C}^{\Omega}$ (Fig. 2). Assume that the body is subjected to a surface traction corresponding to a uniform stress $\boldsymbol{\sigma}_0$. Due to the presence of inclusion in the body, the stress tensor $\boldsymbol{\sigma}$ and strain tensor $\boldsymbol{\varepsilon}$ can be expressed as

$$\boldsymbol{\sigma}(\mathbf{x}) = \boldsymbol{\sigma}^d(\mathbf{x}) + \boldsymbol{\sigma}_0 \tag{2}$$

$$\boldsymbol{\varepsilon}(\mathbf{x}) = \boldsymbol{\varepsilon}^d(\mathbf{x}) + \boldsymbol{\varepsilon}_0 \tag{3}$$

where $\boldsymbol{\varepsilon}_0 = \mathbf{C}^{-1}\boldsymbol{\sigma}_0$, $\boldsymbol{\varepsilon}^d(\mathbf{x})$ and $\boldsymbol{\sigma}^d(\mathbf{x})$ are the disturbance strain and stress fields, respectively. By using Hooke's law, the stress-strain relations in the body can be expressed as follows:

$$\boldsymbol{\sigma}(\mathbf{x}) = \begin{cases} \mathbf{C}(\boldsymbol{\varepsilon}^d(\mathbf{x}) + \boldsymbol{\varepsilon}_0) & \text{for } \mathbf{x} \in V - \Omega \\ \mathbf{C}^{\Omega}(\boldsymbol{\varepsilon}^d(\mathbf{x}) + \boldsymbol{\varepsilon}_0) & \text{for } \mathbf{x} \in \Omega \end{cases} \tag{4}$$

Instead of handling the introduced heterogeneous solid, it is more applicable to deal with an equivalent homogeneous body with the uniform elasticity tensor $\mathbf{C}$. In order to consider the mismatch of the material properties of the matrix and inclusion, it is necessary to define an eigenstrain $\boldsymbol{\varepsilon}^*(\mathbf{x})$ in Ω, such that the equivalent homogeneous solid has the same strain and stress fields as the actual heterogeneous solid under the applied traction. The eigenstrain is given by

$$\boldsymbol{\varepsilon}^*(\mathbf{x}) = \begin{cases} 0 & \text{for } \mathbf{x} \in V - \Omega \\ \boldsymbol{\varepsilon}^* & \text{for } \mathbf{x} \in \Omega \end{cases} \tag{5}$$

Therefore, the stress-strain relation is

$$\boldsymbol{\sigma}(\mathbf{x}) = \mathbf{C}(\boldsymbol{\varepsilon}^d(\mathbf{x}) + \boldsymbol{\varepsilon}_0 - \boldsymbol{\varepsilon}^*) \tag{6}$$

The schematic representation of the homogenization process is depicted in Fig. 2.

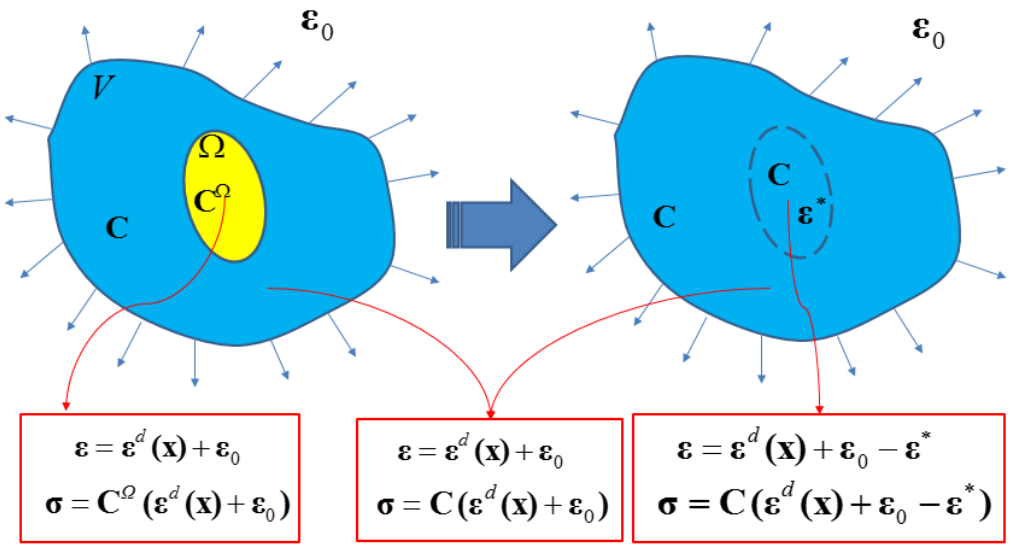

Fig. 2. Illustration of the homogenization process

Eshelby [32] showed that if $V - \Omega$ is homogeneous, linearly elastic, infinitely extended and Ω is an ellipsoid then the eigenstrain, $\boldsymbol{\varepsilon}^*$, and the resulting strain, $\boldsymbol{\varepsilon}^d$, are uniform in Ω. Furthermore, it was shown that the relation between $\boldsymbol{\varepsilon}^d$ and $\boldsymbol{\varepsilon}^*$ is

$$\boldsymbol{\varepsilon}^{\mathbf{d}} = \mathbf{S}^\Omega \boldsymbol{\varepsilon}^* \tag{7}$$

where $\mathbf{S}^\Omega$ is called Eshelby's tensor. This tensor is fourth-order tensor and depends on the geometry and orientation of the inclusion and the elastic properties of the surrounding medium. The components of Eshelby's tensor are given for various inclusion shapes in the literature [33-37]. The components of $\mathbf{S}^\Omega$ for spherical inclusion are expressed by [31]

$$S^\Omega_{ijkl} = \frac{5\nu - 1}{15(1-\nu)}\delta_{ij}\delta_{kl} + \frac{4 - 5\nu}{15(1-\nu)}(\delta_{ik}\delta_{jl} + \delta_{il}\delta_{jk}) \tag{8}$$

where ν is the Poisson ratio of the matrix.

3.2. Generalization of Eshelby's Results

Nemat-Nasser and Hori [31] developed a general form of Eshelby results for a multi-layer inclusion, which each layer has distinct constant eigenstrains. Consider an unbounded uniform elastic solid Ω_1 with an ellipsoidal multi-layer inclusion

E, which contains a nested series of ellipsoids, Ω_α $(\alpha = 2,...m)$ with eigenstrain $\boldsymbol{\varepsilon}^*_\alpha$, such that $\Omega_2 \subset \Omega_3 ....\subset \Omega_m$ and $\Omega_m = E$. Furthermore, annular region between Ω_i and Ω_{i-1} is denoted by $\Gamma_i \equiv \Omega_i - \Omega_{i-1}$ $(i = 3,...m)$ (Fig. 3).

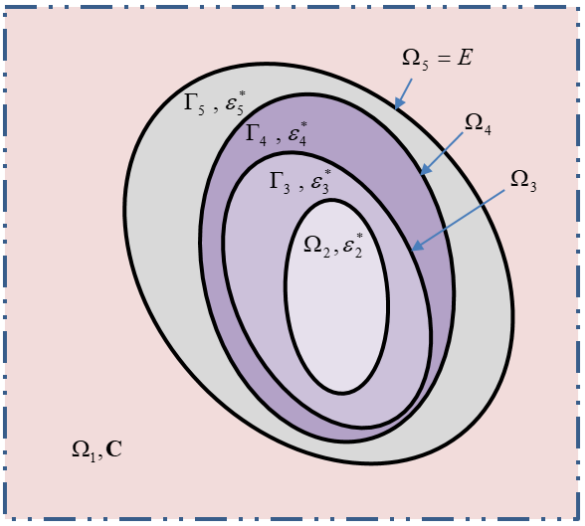

Fig. 3. A four-layer inclusion embedded in an infinite domain

By using Tanaka-Mori result [38], Nemat-Nasser and Hori [31] calculated the volume average strain, $\overline{\boldsymbol{\varepsilon}^d_\alpha}$ in each region. Their proposed relation is somehow complicated but it can be simplified for some special cases. For example, if all Ω_α are similar and coaxial, $\overline{\boldsymbol{\varepsilon}^d_\alpha}$ is only dependent on $\boldsymbol{\varepsilon}^*_\alpha$. i.e.,

$$\overline{\boldsymbol{\varepsilon}^d_\alpha} = \mathbf{S}\boldsymbol{\varepsilon}^*_\alpha \qquad \text{for } \alpha = 2,...m \tag{9}$$

where $\mathbf{S}$ is the common Eshelby tensor of all Ω_α.

3.3. Concentration Tensor

The volume average stress, $\overline{\boldsymbol{\sigma}}$, and volume average strain, $\overline{\boldsymbol{\varepsilon}}$, in a composite with "n" phases can be written as:

$$\overline{\boldsymbol{\sigma}} = \sum_{\alpha=1}^{n} f_a \overline{\boldsymbol{\sigma}}_\alpha \tag{10}$$

$$\overline{\boldsymbol{\varepsilon}} = \sum_{\alpha=1}^{n} f_a \overline{\boldsymbol{\varepsilon}}_\alpha \tag{11}$$

where $\overline{\boldsymbol{\sigma}}_\alpha$ and $\overline{\boldsymbol{\varepsilon}}_\alpha$ are the volume average stress and strain in phase α, and f_a is the volume fraction of each phase, defined as:

$$f_\alpha = \frac{\Omega_\alpha}{V} \tag{12}$$

in which Ω_α is the volume of phase α and V is the volume of the entire composite. If all phases are homogeneous and elastic, the constitutive equations for each phase and the composite are

$$\bar{\boldsymbol{\sigma}}_\alpha = \mathbf{C}_\alpha \bar{\boldsymbol{\varepsilon}}_\alpha \tag{13}$$

$$\bar{\boldsymbol{\sigma}} = \bar{\mathbf{C}}\bar{\boldsymbol{\varepsilon}} \tag{14}$$

where $\mathbf{C}_\alpha$ and $\bar{\mathbf{C}}$ are the elasticity tensors of phase α and the composite, respectively. In this mean-field homogenization scheme, the average strain fields in each phase and the composite are related as follows:

$$\bar{\boldsymbol{\varepsilon}}_\alpha = \mathbf{A}_\alpha \bar{\boldsymbol{\varepsilon}} \tag{15}$$

in which $\mathbf{A}_\alpha$ denotes strain concentration tensor. Using Eqs. (11) and (15), one obtains

$$\mathbf{I} = \sum_{\alpha=1}^{n} f_\alpha \mathbf{A}_\alpha \tag{16}$$

where **I** is the unity tensor. Finally, the effective elasticity tensor of the composite can be obtained by using Eqs. (10)-(16) [39]:

$$\bar{\mathbf{C}} = \mathbf{C}_1 + \sum_{\alpha=1}^{n} f_\alpha (\mathbf{C}_\alpha - \mathbf{C}_1)\mathbf{A}_\alpha \tag{17}$$

In order to obtain the effective moduli of an "*n*" phase composite, the concentration tensor should be determined. In the following section, the procedure for calculating the concentration tensor for a non-dilute composite with multi-layer inclusions will be presented.

3.4. Extension of the Mori-Tanaka Micromechanics Model

In this section, to calculate the concentration tensor for a non-dilute composite having multi-layer inclusions, first, the composite with dilute concentration of inclusions is considered and then by using the Mori-Tanaka assumption, the tensor is modified for the non-dilute dispersion of inclusions.

3.4.1. Effective Elasticity Tensor for a Composite with Multi-Layer Inclusion and Dilute Concentration

An unbounded uniform elastic solid Ω_1 with elasticity tensor $\mathbf{C}_1$ is considered. It encloses an ellipsoidal multi-layer inclusion *E*, containing a nested series of ellipsoids, Ω_α $(\alpha = 2,...m)$, such that $\Omega_2 \subset \Omega_3 ....\subset \Omega_m$ and $\Omega_m = E$ (Fig. 4). The elasticity tensor in various regions of composite is expressed by

$$\mathbf{C}=\mathbf{C}(\mathbf{x})=\begin{cases}\mathbf{C}_1 & if\ \ \mathbf{x}\ in\ \Omega_1\\ \mathbf{C}_2 & if\ \ \mathbf{x}\ in\ \Omega_2\\ \mathbf{C}_\alpha & if\ \ \mathbf{x}\ in\ \Gamma_\alpha\end{cases} \tag{18}$$

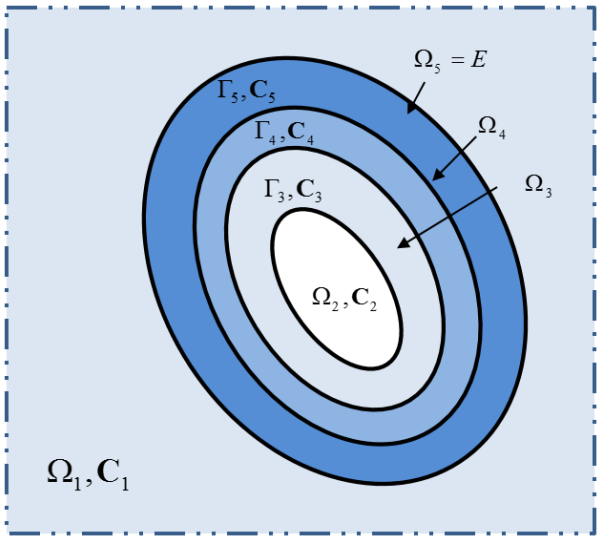

Fig. 4. A four-layer inclusion embedded in an infinite domain Ω_1.

To obtain an equivalent homogenous body with elasticity tensor $\mathbf{C}_1$, we must define $\bar{\boldsymbol{\varepsilon}}_2^*$ and $\bar{\boldsymbol{\varepsilon}}_\alpha^*$ in Ω_2 and Γ_α ($\alpha = 3,...m$), respectively. Therefore, the consistency conditions for the homogenization process are

$$\mathbf{C}_\alpha(\boldsymbol{\varepsilon}_0+\bar{\boldsymbol{\varepsilon}}_\alpha^d)=\mathbf{C}_1(\boldsymbol{\varepsilon}_0+\bar{\boldsymbol{\varepsilon}}_\alpha^d-\bar{\boldsymbol{\varepsilon}}_\alpha^*) \qquad \text{for } \alpha=2,...m \tag{19}$$

If all $\boldsymbol{\Omega}_\alpha$ are similar and coaxial, Eq. (9) holds true. By introducing Eq. (9) into Eq. (19), we obtain the eigenstrain in each region in terms of far field strain $\boldsymbol{\varepsilon}_0$.

$$\bar{\boldsymbol{\varepsilon}}_\alpha^*=\left(\mathbf{B}_\alpha-\mathbf{S}\right)^{-1}\boldsymbol{\varepsilon}_0 \qquad \text{for } \alpha=2,...m \tag{20}$$

where

$$\mathbf{B}_\alpha=\left(\mathbf{C}_1-\mathbf{C}_\alpha\right)^{-1}\mathbf{C}_1 \tag{21}$$

Finally, the strain in each region can be obtained as a function of $\boldsymbol{\varepsilon}_0$, i.e.,

$$\bar{\boldsymbol{\varepsilon}}_\alpha=\boldsymbol{\varepsilon}_0+\bar{\boldsymbol{\varepsilon}}_\alpha^d=\left(\mathbf{I}+\mathbf{S}\left(\mathbf{B}_\alpha-\mathbf{S}\right)^{-1}\right)\boldsymbol{\varepsilon}_0 \tag{22}$$

Comparing Eq. (22) with Eq. (15) and noting that $\bar{\boldsymbol{\varepsilon}}=\boldsymbol{\varepsilon}_0$, the concentration tensor can be obtained as follows:

$$\mathbf{A}_{\alpha}^{dil} = \mathbf{I} + \mathbf{S}\left(\mathbf{B}_{\alpha} - \mathbf{S}\right)^{-1} \tag{23}$$

Consequently, the elasticity tensor for a composite with dilute concentration of multi-layer inclusion can be obtained as follow:

$$\overline{\mathbf{C}} = \mathbf{C}_1 + \sum_{\alpha=1}^{n} f_{\alpha}(\mathbf{C}_{\alpha} - \mathbf{C}_1)\mathbf{A}_{\alpha}^{dil} \tag{24}$$

3.4.2. Effective Elasticity Tensor for a Composite with Multi-Layer Inclusions and Non-Dilute Concentration

In the preceding section, the effect of other inclusions in the stress and strain field is neglected because it is assumed that the multi-layer inclusion is embedded in an infinite matrix. The effect of other inclusions can be accounted by using the Mori-Tanaka approach. In this approach, it is assumed that each inclusion in a non-dilute composite feels the effect of surrounding matrix strain ($\overline{\boldsymbol{\varepsilon}_1}$) in the same way as a single inclusion embedded in an infinite matrix feels a far field strain equals to $\overline{\boldsymbol{\varepsilon}_1}$ (see, Fig. 5).

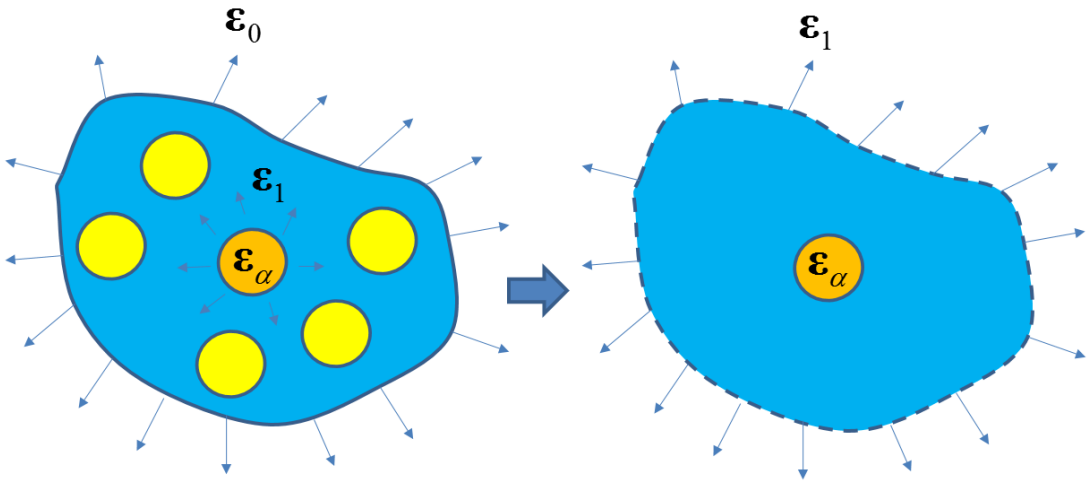

Fig. 5. Schematic of Mori-Tanaka assumption

To apply the Mori-Tanaka assumption in our formulation, we just need to substitute $\bar{\boldsymbol{\varepsilon}}$ in Eq. (24) with $\overline{\boldsymbol{\varepsilon}_1}$. This reformulation is inspired from a study conducted by Dunn and Ledbetter. Accordingly, $\overline{\boldsymbol{\varepsilon}_\alpha}$ in each phase becomes

$$\overline{\boldsymbol{\varepsilon}_\alpha} = \mathbf{A}_{\alpha}^{dil}\overline{\boldsymbol{\varepsilon}_1} = \mathbf{A}_{\alpha}\bar{\boldsymbol{\varepsilon}} = \mathbf{A}_{\alpha}\boldsymbol{\varepsilon}_0 \quad \text{for } \alpha = 2,...m \tag{25}$$

Then, according to Eq. (11), we have

$$\boldsymbol{\varepsilon_0} = \bar{\boldsymbol{\varepsilon}} = \sum_{\alpha=1}^{n} f_\alpha \overline{\boldsymbol{\varepsilon}_\alpha} = \left(f_1 \mathbf{I} + \sum_{\alpha=2}^{n} f_\alpha \mathbf{A}_\alpha^{dil} \right) \overline{\boldsymbol{\varepsilon}_1} \tag{26}$$

So, the concentration tensor for a non-dilute composite with multi-layer inclusions obtains as follows:

$$\mathbf{A}_\alpha = \mathbf{A}_\alpha^{dil} \left(f_1 \mathbf{I} + \sum_{\alpha=2}^{n} f_\alpha \mathbf{A}_\alpha^{dil} \right)^{-1} \quad \text{for } \alpha = 2,...m \tag{27}$$

Finally, the relation for the stiffness tensor of a non-dilute composite with multi-layer inclusions is expressed as

$$\begin{aligned} \overline{\mathbf{C}} &= \mathbf{C}_1 + \sum_{\alpha=2}^{n} f_\alpha (\mathbf{C}_\alpha - \mathbf{C}_1) \mathbf{A}_\alpha^{dil} \left(f_1 \mathbf{I} + \sum_{\alpha=2}^{n} f_\alpha \mathbf{A}_\alpha^{dil} \right)^{-1} \\ &= \mathbf{C}_1 + \sum_{\alpha=2}^{n} f_\alpha (\mathbf{C}_\alpha - \mathbf{C}_1) \left(\mathbf{I} + \mathbf{S} \left(\mathbf{B}_\alpha - \mathbf{S} \right)^{-1} \right) \left(f_1 \mathbf{I} + \sum_{\alpha=2}^{n} f_\alpha \left(\mathbf{I} + \mathbf{S} \left(\mathbf{B}_\alpha - \mathbf{S} \right)^{-1} \right) \right)^{-1} \end{aligned} \tag{28}$$

Equation (28) is the extension of the Mori-Tanaka model for a composite with multi-layer inclusions. Therefore, we call this new model "*Extended Mori-Tanaka Micromechanics Model*".

3.5. Extension of the Halpin-Tsai Model

In this subsection, we attempted to extend the Halpin–Tsai model for a multi-phase composite. Halpin and Tsai [40] developed a semi-empirical model based on the works done by Hill [41] and Hermans [42]. The model was developed for two-phase composite. The common form of the Halpin–Tsai equation has the following form

$$\frac{\overline{E}}{E_m} = \frac{1 + \xi \eta \varphi}{1 - \eta \varphi} \quad \text{with } \eta = \frac{E_f - E_m}{E_f + \xi E_m} \tag{29}$$

where $\overline{E}$, E_m and E_f are Young's moduli of the composite, the matrix and the reinforcement, respectively, and φ is the volume fraction of reinforcement. Furthermore, in Eq. (29), ξ is an empirical parameter and is a measure of reinforcement geometry which depends on the loading conditions. This parameter is usually determined by curve fitting of experimental or numerical data [43]. We propose the extended Halpin-Tsai model for a multi-phase composite as follows:

$$\frac{\overline{E}}{E_m} = \frac{1 + \xi \sum_\alpha \eta_\alpha f_\alpha}{1 - \sum_\alpha \eta_\alpha f_\alpha} \tag{30}$$

in which f_α is the volume fraction of phase α and η_α is defined by

$$\eta_\alpha = \frac{E_\alpha - E_m}{E_\alpha + \xi E_m} \tag{31}$$

where E_α is Young's modulus of phase α .

4. Results and discussion

In this section, Young's modulus of FRPCs with different weight fractions of the C_{60} are calculated from the Extended Mori-Tanaka, extended Halpin-Tsai models and the results are compared with the results of MD simulations.

4.1. Two-phase models

To elucidate the importance of considering multi-phase composite models for modeling the FRPCs, in the first subsection, we only consider two phases in each RVE (Fig. 6). In this case, since we have two-phase composite, the common form of Mori-Tanaka and Halpin-Tsai models are used to predict the Young modulus. The results obtained from these micromechanics models are listed in Table 3 and are compared with the MD results.

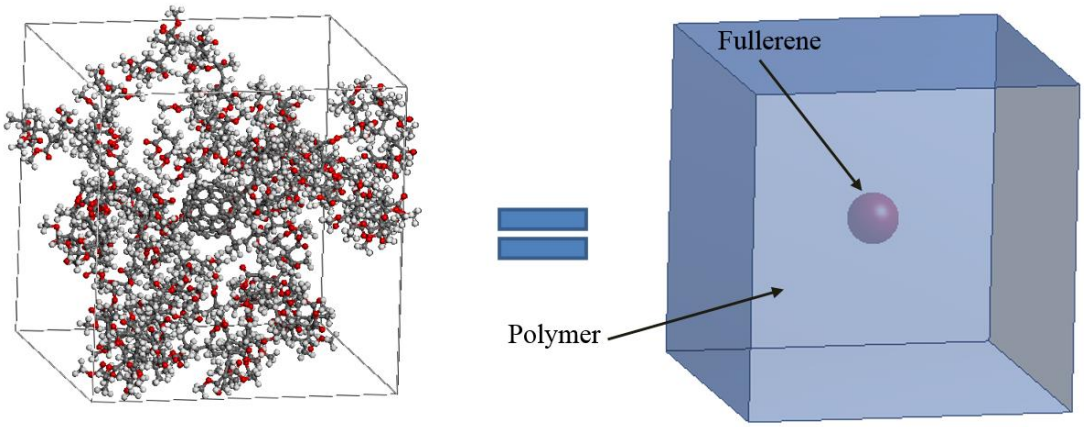

Fig. 6. Molecular unit cell and the two-phase equivalent continuum model

Table 3. Elastic modulus of FRPCs obtained from the MD simulations, and two phase Mori-Tanaka and Halpin-Tsai models

Weight fractions	Young's Modulus (GPa)		
	MD simulation	Mori-Tanaka model	Halpin-Tsai model
1	3.298	3.0100	3.0147
2	3.313	3.0202	3.0297
3	3.438	3.0304	3.0447
4	3.774	3.0413	3.0607

As can be inferred from the table, by considering two phases for the FRPC, all of micromechanics models fail to predict to the MD simulation results. This clearly reveals the importance of considering the interphase region on the calculation of

elastic properties of FRPCs. A similar conclusion has previously been reported for carbon nanotube-reinforced polymer nanocomposites [44].

4.2. Multi-phase models

In this subsection, the extended Mori-Tanaka and extended Halpin-Tsai models are used to predict the results of the MD simulations. Two different cases are investigated: 1) four-phase model comprising the fullerene (solid sphere), the interface region, the interphase region, and the polymer, and 2) five-phase model comprising an internal void in fullerene, the fullerene (Spherical shell), the interface region, the interphase region, and the polymer (Fig. 7). In Table 4, the volume fractions of different phases in the four-phase model is presented. As inferred from Table 4, the volume fraction of the interphase region is about 68 times higher than C_{60} and 20 times higher than the interface in each unit cell. So, it is physically a more dominant layer than the two other phases. Similar results in the literature emphasize the role of interphase as the true reinforcement phase in carbon-based nanocomposite [12, 25, 44]. Due to the soft interface, the load transfer from the matrix to the fullerene is deemed weak, and hence Young's modulus of the interface is set to zero. Furthermore, Young's modulus of internal void is set to zero since no atom is present in this region. In addition, the empirical parameter ξ is set to 2 which is the value suggested for spherical inclusion [45].

Table 4. Volume fractions of different phases in the four-phase model

Weight fraction of C_{60}	Volume Fractions			
	Fullerene	Interface	Interphase	Matrix
1	0.0016	0.0056	0.1116	0.8812
2	0.0033	0.0113	0.2255	0.7599
3	0.005	0.0169	0.3384	0.6398
4	0.0067	0.0229	0.4586	0.5118

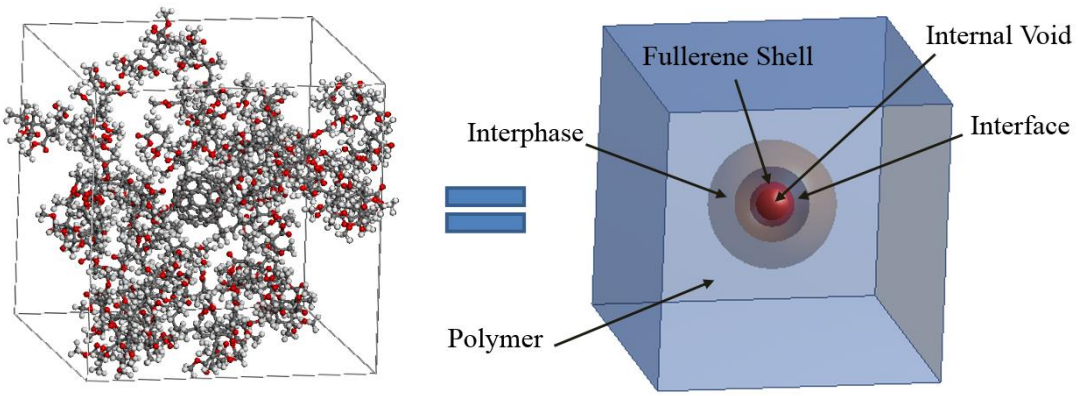

Fig. 7. Molecular unit cell and the five-phase equivalent continuum model

The computed values of the Young modulus of the C_{60}/PMMA nanocomposites with various weight fractions are listed in Table 5 for the two different cases. As can be seen from Table 5, the extended Mori-Tanaka model can successfully predict the MD simulation results. This clearly shows the capability of the model in describing the stiffening mechanism of fullerene molecule in the polymer composite. Furthermore, it is observed that the results of the five-phase model are more closed to the MD simulation results. In addition, the results reveal that extended Halpin-Tsai model can predict acceptable results.

Table 5. Comparison of Young's modulus calculated from extended Mori-Tanaka and extended Halpin-Tsai models with the MD simulation results

Weight fractions	Young's Modulus (GPa)				
	MD simulation	Extended Mori-Tanaka model		Extended Halpin-Tsai model	
		Four-phase	Five-phase	Four-phase	Five-phase
1	3.298	3.182	3.194	3.207	3.221
2	3.313	3.321	3.347	3.372	3.399
3	3.438	3.465	3.505	3.540	3.584
4	3.774	3.625	3.682	3.726	3.788

5. Conclusions

In this paper, an extended Mori-Tanaka model for composites with multi-layer inclusions was developed to estimate Young's modulus of FRPNs with different weight fractions. Furthermore, an extension to Halpin-Tsai model was proposed to account the multi-layer inclusions in composites. First, the Young moduli of composite and the effective interphase were computed by the MD simulations. Then, for comparison purposes, the common Mori–Tanaka and the Halpin-Tsai micromechanics models were used to calculate the Young modulus of the FRPNs. A comparison of the two-phase micromechanical results and the MD results indicates that the Young modulus of the nanocomposites cannot be precisely predicted using the two-phase micromechanical models which proves the indispensable role of interphase region in the reinforcement of nanocomposite. The results of multi-phase micromechanical models were computed and compared with the MD results. The results clearly revealed the capability of the four- and five-phase models to predict Young's modulus of FRPNs. It can be concluded that the accuracy of results depends on two main parameters: the number of phase and accuracy of estimating of the Young modulus of each phase. Finally, the micromechanical models proposed herein can be utilized to predict Young's modulus of composites with inclusions possessing arbitrary number of layers.

Conflict of interest

The authors declare that there are no conflicts of interest.

References

[1] Zeng, Q., Yu, A., Lu, G., 2008. Multiscale modeling and simulation of polymer nanocomposites. Progress in Polymer Science 33, 191-269.

[2] Okonkwo, A.O., Jagadale, P., Herrera, J.E.G., Hadjiev, V.G., Saldaña, J.M., Tagliaferro, A., Hernandez, F.C.R., 2015. High-toughness/low-friction ductile epoxy coatings reinforced with carbon nanostructures. Polymer Testing 47, 113-119.

[3] Moghaddam, F., Ghavanloo, E., Fazelzadeh, S.A., 2016. Effect of carbon nanotube geometries on mechanical properties of nanocomposite via nanoscale representative volume element. Journal of Solid Mechanics, 8, 568-577.

[4] Zaccardi, F., Santonicola, M.G., Laurenzi, S., 2021. Role of interface bonding on the elastic properties of epoxy-based nanocomposites with carbon nanotubes using multiscale analysis. Composite Structures, 255, 113050.

[5] Calleja, F.B., Giri, L., Asano, T., Mieno, T., Sakurai, A., Ohnuma, M., Sawatari, C., 1996. Structure and mechanical properties of polyethylene-fullerene composites. Journal of Materials Science 31, 5153-5157.

[6] Zhogova, K., Davydov, I., Punin, V., Troitskii, B., Domvachiev, G., 2005. Investigation of fullerene C_{60} effect on properties of polymethylmethacrylate exposed to ionizing radiation. European Polymer Journal 41, 1260-1264.

[7] Kropka, J.M., Putz, K.W., Pryamitsyn, V., Ganesan, V., Green, P.F., 2007. Origin of dynamical properties in PMMA−C_{60} nanocomposites. Macromolecules 40, 5424-5432.

[8] Ogasawara, T., Ishida, Y., Kasai, T., 2009. Mechanical properties of carbon fiber/fullerene-dispersed epoxy composites. Composites Science and Technology 69, 2002-2007.

[9] Rafiee, M.A., Yavari, F., Rafiee, J., Koratkar, N., 2011. Fullerene–epoxy nanocomposites-enhanced mechanical properties at low nanofiller loading. Journal of Nanoparticle Research 13, 733-737.

[10] Ginzburg, B., Tuichiev, S., Rashidov, D., Tabarov, S.K., Sukhanova, T., Vylegzhanina, M., 2012. Effect of fullerene C_{60} on the structure and mechanical properties of thin films based on poly (methylmethacrylate) and other carbochain vinyl polymers: a technological aspect. Polymer Science Series A 54, 658-670.

[11] Adnan, A., Sun, C., Mahfuz, H., 2007. A molecular dynamics simulation study to investigate the effect of filler size on elastic properties of polymer nanocomposites. Composites Science and Technology 67, 348-356.

[12] Ferdous, S.F., Sarker, M.F., Adnan, A., 2013. Role of nanoparticle dispersion and filler-matrix interface on the matrix dominated failure of rigid C_{60}-PE nanocomposites: a molecular dynamics simulation study. Polymer 54, 2565-2576.

[13] Jeyranpour, F., Alahyarizadeh, G., Minuchehr, A., 2016. The thermo-mechanical properties estimation of fullerene-reinforced resin epoxy composites by molecular dynamics simulation–A comparative study. Polymer 88, 9-18.

[14] Lu, C.T., Weerasinghe, A., Maroudas, D., Ramasubramaniam, A., 2016. A comparison of the elastic properties of graphene-and fullerene-reinforced polymer composites: the role of filler morphology and size. Scientific Reports 6, 31735.

[15] Giannopoulos, G.I., 2019. Linking MD and FEM to predict the mechanical behaviour of fullerene reinforced nylon-12. Composites Part B 161, 455-463.

[16] Izadi, R., Ghavanloo, E., Nayebi, A., 2019. Elastic properties of polymer composites reinforced with C_{60} fullerene and carbon onion: molecular dynamics simulation. Physica B 574, 311636.

[17] Giannopoulos, G.I., Georgantzinos, S.K., Anifantis, N.K., 2020. Thermomechanical response of fullerene-reinforced polymers by coupling MD and FEM. Materials 13, 4132.

[18] Yang, B.J., Shin, H., Lee, H.K., Kim, H., 2013. A combined molecular dynamics/micromechanics/finite element approach for multiscale constitutive modeling of nanocomposites with interface effects. Applied Physics Letters 103, 241903.

[19] Marcadon, V., Brown, D., Hervé, E., Melé, P., Albérola, N.D., Zaoui, A., 2013. Confrontation between Molecular Dynamics and micromechanical approaches to investigate particle size effects on the mechanical behaviour of polymer nanocomposites. Computational Materials Science 79, 495-505.

[20] Shokrieh, M.M., Esmkhani, M., Shokrieh, Z., Zhao, Z., 2014. Stiffness prediction of graphene nanoplatelet/epoxy nanocomposites by a combined molecular dynamics–micromechanics method. Computational Materials Science 92, 444-450.

[21] Hoover, W.G., 1985. Canonical dynamics: Equilibrium phase-space distributions. Physical Review A 31, 1695-1697.

[22] Lin, Y., Pan, D., Li, J., Zhang, L., Shao, X., 2017. Application of Berendsen barostat in dissipative particle dynamics for nonequilibrium dynamic simulation. Journal of Chemical Physics 146, 124108.

[23] Karatrantos, A., Clarke, N., Kröger, M., 2016. Modeling of polymer structure and conformations in polymer nanocomposites from atomistic to mesoscale: a Review. Polymer Reviews 56, 385-428.

[24] Coleman, J.N., Cadek, M., Ryan, K.P., Fonseca, A., Nagy, J.B., Blau, W.J., Ferreira, M.S., 2006. Reinforcement of polymers with carbon nanotubes. The role of an ordered polymer interfacial region. Experiment and modeling. Polymer 47, 8556-8561.

[25] Malagù, M., Goudarzi, M., Lyulin, A., Benvenuti, E., Simone, A., 2017. Diameter-dependent elastic properties of carbon nanotube-polymer composites: Emergence of size effects from atomistic-scale simulations. Composites Part B, 131, 260-281.

[26] Weishaupt, K., Krbecek, H., Pietralla, M., Hochheimer, H., Mayr, P., 1995. Pressure dependence of the elastic constants of poly (methyl methacrylate). Polymer 36, 3267-3271.

[27] Giannopoulos, G., Georgantzinos, S., Kakavas, P., Anifantis, N., 2013. Radial stiffness and natural frequencies of fullerenes via a structural mechanics spring-based method. Fullerenes, Nanotubes and Carbon Nanostructures 21, 248-257.

[28] Jamal-Omidi, M., ShayanMehr, M., Rafiee, R., 2016. A study on equivalent spherical structure of buckyball-C_{60} based on continuum shell model. Latin American Journal of Solids and Structures 13, 1016-1029.

[29] Nayebi, A., Ghavanloo, E., Hosseini, N., 2016. Young's modulus Estimation of fullerene nano-structure by using molecular mechanics and finite element method. Modares Mechanical Engineering 16, 41-48.

[30] Ghavanloo, E., Izadi, R., Nayebi, A., 2018. Computational modeling of the effective Young's modulus values of fullerene molecules: a combined molecular dynamics simulation and continuum shell model. Journal of Molecular Modeling 24, 71.

[31] Nemat-Nasser, S., Hori, M., 1993. Micromechanics :Overall Properties of Heterogeneous Materials. Elsevier.

[32] Eshelby, J.D., 1957. The determination of the elastic field of an ellipsoidal inclusion, and related problems. Proceedings of the Royal Society of London. Series A 241, 376-396.

[33] Kiris, A., Inan, E., 2006. Eshelby tensors for a spherical inclusion in microstretch elastic fields. International Journal of Solids and Structures 43, 4720-4738.

[34] Ma, H., Hu, G., 2007. Eshelby tensors for an ellipsoidal inclusion in a microstretch material. International Journal of Solids and Structures 44, 3049-3061.

[35] Ma, H.M., Gao, X.L., 2010. Eshelby's tensors for plane strain and cylindrical inclusions based on a simplified strain gradient elasticity theory. Acta Mechanica 211, 115-129.

[36] Trotta, S., Marmo, F., Rosati, L., 2017. Evaluation of the Eshelby tensor for polygonal inclusions. Composites Part B 115, 170-181.

[37] Yun, G.J., Zhu, F.Y., Lim, H.J., Choi, H., 2021. A damage plasticity constitutive model for wavy CNT nanocomposites by incremental Mori-Tanaka approach. Composite Structures, 258, 113178.

[38] Tanaka, K., Mori, T., 1972. Note on volume integrals of the elastic field around an ellipsoidal inclusion. Journal of Elasticity 2, 199-200.

[39] Jain, A., Jin, B. C., Nutt, S., 2017. Mean field homogenization methods for strand composites. Composites Part B 124, 31-39.

[40] Halpin, J., Tsai, S., 1969. Effects of environmental factors on composite materials. Air Force Materials Lab Wright-Patterson AFB OH.

[41] Hill, R., 1963. Elastic properties of reinforced solids: some theoretical principles. Journal of the Mechanics and Physics of Solids 11, 357-372.

[42] Hermans, J., 1967. Elastic properties of fiber reinforced materials when fibers are aligned. Koninklijke Nederlandse Akademie Van Weteschappen-Proceedings Series B-Physical Sciences 70, 1.

[43] Raju, B., Hiremath, S.R., Mahapatra, D.R., 2018. A review of micromechanics based models for effective elastic properties of reinforced polymer matrix composites. Composite Structures 204, 607-619.

[44] Amraei, J., Jam, J. E., Arab, B., Firouz-Abadi, R.D., 2019. Modeling the interphase region in carbon nanotube-reinforced polymer nanocomposites. Polymer Composites 40, E1219-E1234.

[45] Affdl, J.H., Kardos, J.L., 1976. The Halpin-Tsai equations: a review. Polymer Engineering & Science 16, 344-352.